

VORTEX RING BELOW A SPREADING ALCOHOL FILM ON WATER

Anurag Pant^{1,*} & Baburaj A. Puthenveetil¹

¹Department Of Applied Mechanics, Indian Institute of Technology Madras,
Chennai, Tamil Nadu, India, 600036

*Address all correspondence to: Anurag Pant, PhD Scholar, Department Of Applied Mechanics, Indian Institute of Technology Madras, Chennai, Tamil Nadu, India, 600036, E-mail: akkupant@gmail.com

We study the expansion of a vortex ring generated due to the spreading of ethanol-water droplets, with ethanol concentration range of $20\% \leq C_e \leq 100\%$, on the surface of a 50 mm deep water layer. Once deposited on the water layer, the surface tension difference leads to some part of the lighter ethanol droplet spreading as a thin film over the water layer. We observe an expanding vortex ring below the radially spreading film front. We visualize the film spreading from top using aluminum particles, while the vortex is visualized from the side using polyamide particles with LIF from the dyed drop used to distinguish the alcohol from the water. PIV is used to obtain the velocity and the vorticity fields below the spreading film. Vortex regions and their centers, identified by the λ_2 method from the velocity fields, are tracked to determine the vortex expansion. We show that the vortex ring expands with the same velocity of expansion as that of the spreading ethanol film at the free surface, possibly since the vortex ring is created due to the surface tension difference across the film front. Using dimensional arguments, we also propose a scaling for the upward velocity, u_Γ , induced by this expanding vortex ring and show that $u_\Gamma \sim t^{-1/2}$.

KEY WORDS: Drops; Spreading; Vortices; PIV; Surface tension

1. INTRODUCTION

A lighter drop of ethanol, when gently placed atop the surface of a deep water layer leads to an interesting display of surface tension driven dynamics. Surface tension difference between the ethanol and water leads to a positive spreading coefficient, which in turn leads to surface tension driven, fast, radial spreading of a film from the floating ethanol drop. We observe an expanding vortex ring below the leading edge of the spreading alcohol film and study its expansion velocity and the upward velocity it induces, in this paper.

The spatial evolution of surfactant laden droplets spreading due to surface tension difference has been studied extensively since they find applications such as drug delivery, imitated by surfactant monolayers spreading on thin viscous films (Jensen and Grotberg (1992)), and oil spills on seas (Fay (1969)). In a study, with coating processes in mind, Hernandez-Sanchez et al. (2015) found that a continuous supply of alcohol on the surface of a thin water film creates a flow similar to that in a hydraulic jump. Multitudes of scaling laws for the radial expansion of films on liquids have been observed. The spreading radius of low viscosity aqueous surfactant films of FC-129, a fluorochemical surfactant, on organic solutions (CCl_4) was found to depend on time as $r_f \sim t^{3/4}$ (Joos and Van Hunsel (1985)), due to the balance between the interfacial and viscous stresses. On the other hand, extremely viscous droplets of PDMS spreading on glycerol-water mixtures show that the drop radius varies as $t^{1/4}$ and $t^{1/2}$ in the capillary and the gravitational regimes respectively (Bacri et al. (1996)). Dussaud and Troian (1998) observe that for an immiscible, volatile droplet spreading on water, the spreading radius varies as $t^{1/2}$.

Dandekar et al. (2017) observed that a miscible, volatile ethanol droplet spreads on a deep water layer with the film spreading radius r_f varying with time t as

$$r_f^* = \frac{1}{f} t_{\mu d}^{*1/4}, \quad (1)$$

where $r_f^* = r_f/r_d$, $t_{\mu d}^* = t/t_{\mu d}$ and

$$f(Bo_d) = \frac{3^{1/4}}{2} (1 + Bo_d)^{3/4}, \quad (2)$$

1 with $t_{\mu d} = \mu_d r_d / \Delta\sigma$, $Bo_d = \rho_d g r_d^2 / \Delta\sigma$ is the drop Bond number, μ_d is the drop viscosity, r_d
2 is the drop radius, $\Delta\sigma$ the surface tension difference and ρ_d the drop density. The above scaling
3 was obtained by the balance of surface tension driven spreading force with the viscous resistance
4 in the film and assumed no mixing of the alcohol film and the underlying fluid.

5 However, a vortex ring, expanding beneath the edge of spreading film has been observed
6 in the studies of a volatile film of toluene spreading on water (Dussaud and Troian (1998)), iso-
7 propyl alcohol film on water in HeleShaw cells (Kim et al. (2015)) and by Dandekar et al. (2017).
8 Figure 1 shows the schematic of a vortex ring beneath a spreading ethanol film. The role of these
9 vortices that form below spreading films above liquid substrates, in deciding the spreading dy-
10 namics of the film, is not known. The origin of such vortices is also not known clearly. Such
11 vortices could lead to the mixing of the spreading liquid in the film with the substrate fluid at the
12 later stages of spreading of the film. In this paper, we study the vortical flow below the spreading
13 film of a miscible, volatile liquid on a liquid substrate, namely ethanol film on water. We present
14 particle based flow visualizations of the film spreading from the top. Side view visualizations
15 using particles and LIF of the dye laden drop in the region underneath the spreading drop are
16 also studied, which show the signature of an axisymmetric vortex ring in the form of two counter
17 rotating vortices. The velocity and vorticity fields in a vertical plane below the spreading film
18 are obtained using PIV. The vortices are identified, and their positions tracked, by applying the
19 λ_2 criterion, (Jeong and Hussain (1995)) on the velocity field. The scalings for the velocity of
20 expansion of the axisymmetric vortex ring, and the upward velocity induced by this vortex ring
21 are then obtained.

22 2. EXPERIMENTS

23 The following experiments were conducted to study the spreading of an ethanol droplet on the
24 water surface and the vortex ring expansion below it. Hereinafter, the subscripts d denote the
25 drop, f the spreading film, and e the ethanol.

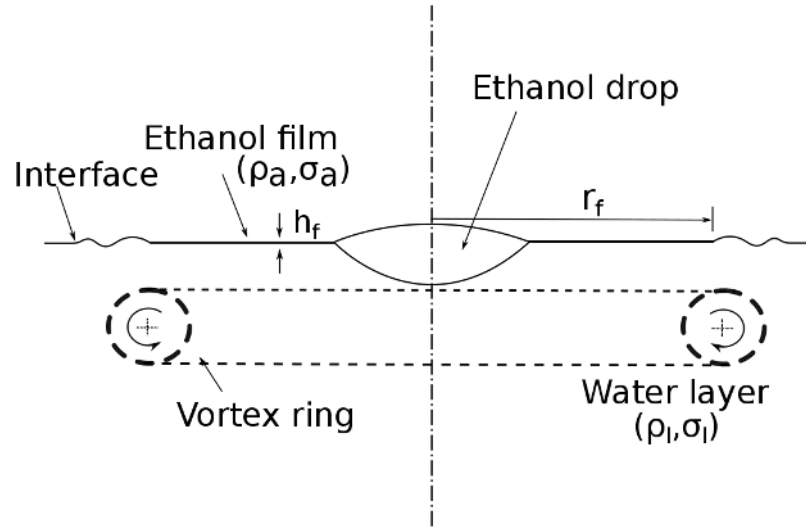


FIG. 1: Schematic of film spreading from a drop of ethanol over water with an expanding vortex ring below the outer periphery of the expanding film. Major part of the drop floats at the center before eventually getting mixed.

1 2.1 Top view visualization

2 Top view visualizations were conducted with an ethanol drop of $r_d=0.97\text{mm}$ and ethanol con-
 3 centration $C_e=80\%$ deposited on a 75 mm water layer to study the film spreading. Aluminum
 4 particles floating at the free surface were used for these visualizations. A particle size analyzer
 5 (Microtrac Inc) was used to determine the particle size. The aluminum particles were found to
 6 have a median diameter of $14.65\ \mu\text{m}$ and a mean diameter of $5.09\ \mu\text{m}$. The images were captured
 7 using a high-speed camera (LaVision ProHS) at approximately 300 f.p.s with LED backlight-
 8 ing. Figure 2 shows the outcome of such a visualization where the spreading alcohol film with a
 9 radius r_f is seen as the particle free circular region.

10 2.2 Side view visualization

11 Side view visualizations to study the coalescence dynamics were done in a glass tank measuring
 12 $50\text{mm}\times 50\text{mm}\times 50\text{mm}$ with an ethanol drop of $r_d=1.1\text{mm}$ and $C_e=100\%$ placed on a 50mm
 13 water layer. The drop was tagged with $6\ \mu\text{m}$ fluorescent particles and the substrate contained

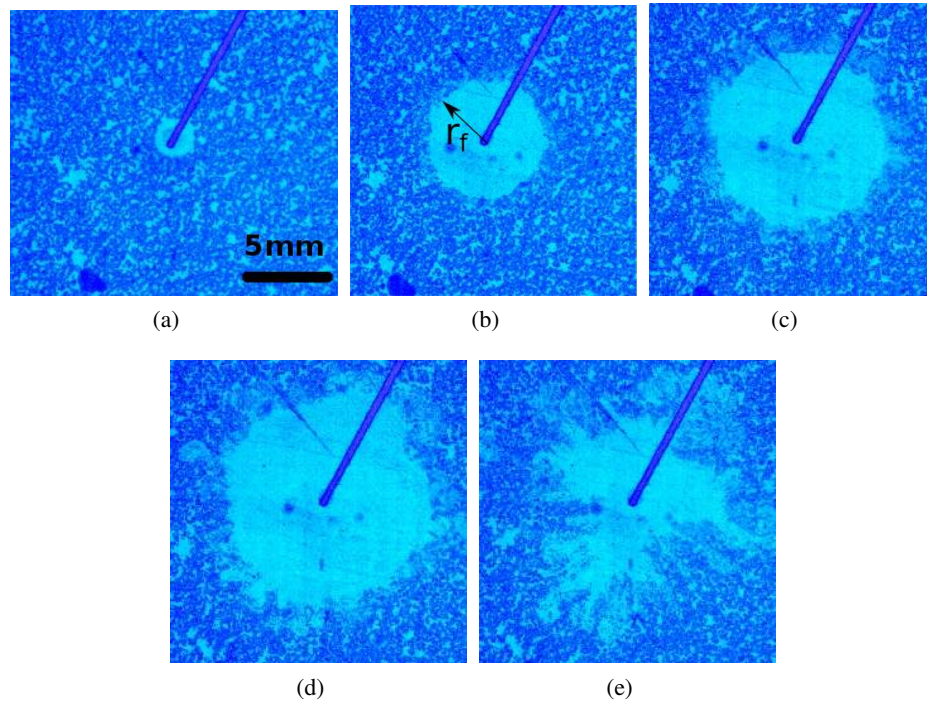


FIG. 2: Top view of the spreading film visualized using aluminum particles for the case of $r_d = 0.97$ mm and $C_e = 80\%$ when an ethanol drop is deposited on a 75 mm deep water layer at (a), $t = 0$ ms; (b), $t = 50$ ms; (c), $t = 100$ ms; (d), 150 ms and (e), 217 ms.

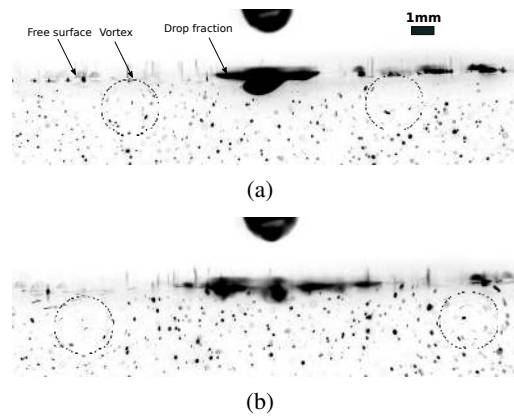


FIG. 3: Side view of the spreading dynamics visualized using $55 \mu\text{m}$ polyamide particles in the water layer and $6 \mu\text{m}$ fluorescent particles in the ethanol drop for the case of $r_d = 1$ mm, $C_e = 100\%$ deposited on a 50 mm deep water layer at (a), 40 ms and (b), 80 ms. The original images have been inverted for clarity and shown above. The dashed circles show an expanding vortex ring beneath the tip of the spreading film.

1 55 μ m polyamide particles. In some cases, the drop contained 0.1ppm of Rhodamine 6G dye so
2 that the ethanol region could be distinguished from the water region. A thin laser sheet from a
3 2W, 532nm solid state laser was made to pass through the drop center. The images were captured
4 at 500 f.p.s using a Photron SA5 camera where the fluorescent particles in the drop and the
5 film fluoresced due to LIF(Laser induced fluorescence) while the polyamide particles in the
6 water scattered the light. The motive behind the side view visualizations was to qualitatively
7 understand the role of coalescence dynamics, that occur when the drop touches the water surface,
8 in the subsequent spreading of the ethanol film. The dynamics in the bulk could also be studied
9 in these visualizations. Figure 3 shows an example such a side view visualization where the
10 spreading film and the vortex ring could be identified.

11 **2.3 PIV measurements**

12 PIV experiments to study the dynamics of the vortex ring were conducted in a glass tank of size
13 100mm \times 100mm \times 50 mm. Water, containing seeding particles(Polyamide, 55 μ mean diameter,
14 1.03 g/cm³ density, Lavision GmbH), was filled up to the brim of the tank to avoid meniscus
15 effects while visualizing. Needles of different sizes were connected to a syringe pump and posi-
16 tioned at the center of the glass tank above the free surface, with the flow rates of water-alcohol
17 solutions kept at a low value (2.4 ml/h), so as to have periodic dripping of alcohol drops of
18 specific sizes. The drop radius was calculated by counting the number of drops that fill a given
19 volume. Figure 4 shows the schematic of the experimental set up used for PIV.

20 A vertical laser sheet pulse of 1mm thickness with 80mJ/pulse (532nm, Nd:YAG laser,Litron)
21 was passed parallel to the tank walls. It was positioned in such a way that it illuminated a plane
22 passing through the drop center. The drop was brought very close to the surface and then made
23 to detach in order to avoid inertial effects due to its impingement. The particle images in the wa-
24 ter layer were then captured using a high speed CCD camera(Imager Pro HS, Lavision GmbH)
25 positioned perpendicular to the plane illuminated by the laser sheet. It was made sure that the
26 depth of field of the camera exceeded the laser sheet thickness so that all the particles in the laser
27 sheet were in focus. The separation between the two laser pulses was set so that the out of plane

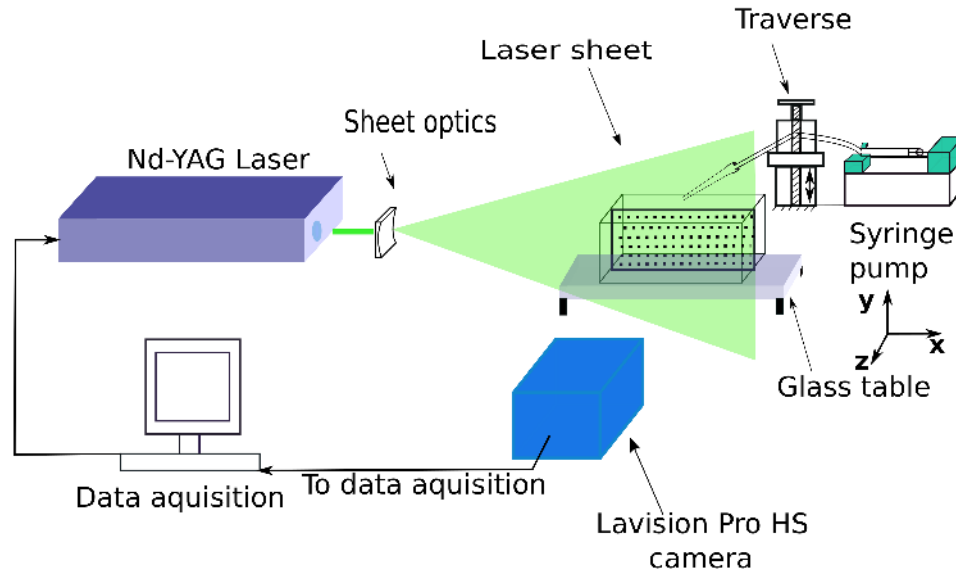


FIG. 4: Schematic of the experimental setup

1 displacement of particles was less than one-fourth of the sheet thickness (Adrian and Westerweel
 2 (2011)). The images were recorded at 50 Hz. The above steps were performed for drops with C_e
 3 ranging from 20% to 100%. The concentrations of alcohol in the drop (C_e), their surface tension
 4 values (σ), kinematic viscosity values (ν) and densities (ρ) are shown in Table 1.

5 The particle images were processed using an adaptive multi pass cross correlation algorithm
 6 that uses fast Fourier transform (FFT) and zero-padding in DAVIS (Lavisision GmbH). A window

Ethanol concentration(C_e) (%)	Surface tension(σ) (Nm)	Surface tension difference($\Delta\sigma$) (Nm)	Kinematic viscosity(ν) (m^2/s)	Density(ρ) (kg/m^3)
20	37.97	34.03	1.76	970.36
40	31.00	41.00	2.34	948.47
60	26.00	46.00	2.24	908.72
80	23.80	48.20	1.66	859.58
100	22.00	50.00	1.10	790.74

TABLE 1: Properties of the various ethanol-water solutions used in the drop. The values for different concentrations at 25°C were obtained from Ernst et al. (1935).

a

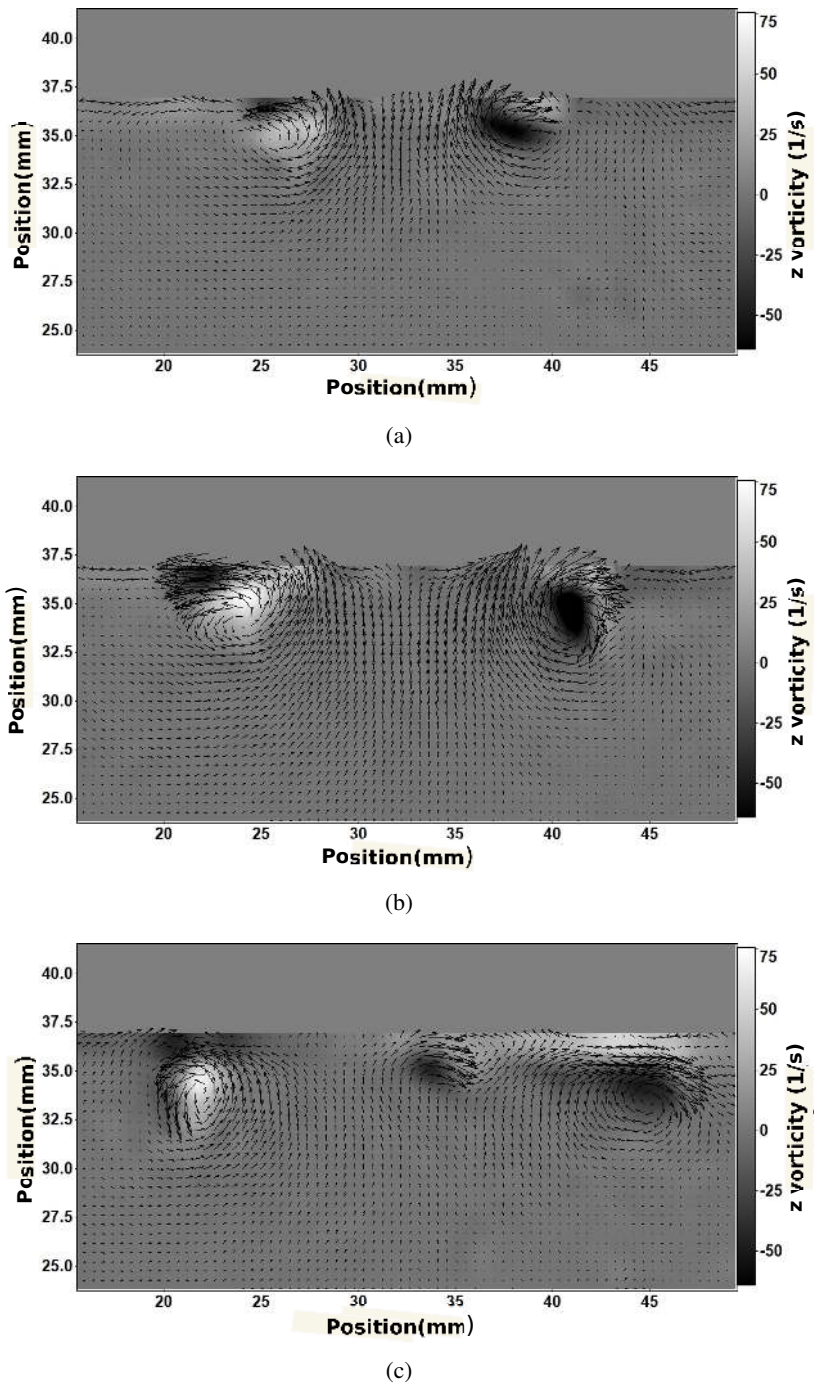


FIG. 5: Velocity fields in a vertical plane overlaid with the vorticity field at various times for a 1 mm droplet of $C_e = 100\%$ deposited on a 50 mm deep water layer at (a), $t = 80$ ms; (b), $t = 240$ ms and (c), $t = 400$ ms.

1 size of 16×16 pixel was chosen with 50 % overlap in order to obtain the velocity field. There
 2 were 6-7 vectors across the vortex core diameter with a pixel size of 0.06 mm/pixel. The corre-
 3 lation peaks were interpolated using three-point one-dimensional Gaussian peak fitting. Image
 4 correction was performed to ensure that any inhomogeneity in illumination of particles was re-
 5 moved before processing the data in order to reduce spurious vectors. These steps were followed
 6 by the single pass of a median filter to further reduce the spurious vectors. The velocity fields
 7 thus obtained, for the case of $r_d = 1.1$ mm and $C_e = 80\%$, is shown in Figure 5 at various times.
 8 The uncertainties in these velocities were calculated using the correlation statistics method of
 9 Wieneke (2015) available in DAVIS (Lavisision GmbH).

10 2.4 Vortex core identification

11 In order to track the expansion of the vortex ring generated as a result of the film spreading
 12 on the surface, we needed to identify the vortex and its center from the 2D PIV vector fields.
 13 Amongst the many available methods of vortex identification, such as the λ_2 method by Jeong
 14 and Hussain (1995), Q criterion by Hunt (1988), Δ criterion by Chong et al. (1990), swirling
 15 strength criterion by Zhou et al. (1999) and that of Agrawal and Prasad (2002), we chose the λ_2
 16 method to identify the vortex core. The velocity vector field was obtained using the PIVMat 4.10
 17 toolbox, from which the 2D velocity gradient tensor,

$$J = \nabla U = \begin{bmatrix} \frac{\partial u}{\partial x} & \frac{\partial u}{\partial y} \\ \frac{\partial v}{\partial x} & \frac{\partial v}{\partial y} \end{bmatrix}, \quad (3)$$

18 was calculated for each point in the velocity field. J was then decomposed into symmetric and
 19 antisymmetric parts, $S = (J + J^T)/2$ and $\Omega = (J - J^T)/2$ respectively. The eigen values of
 20 $S^2 + \Omega^2$ were calculated such that for each point in the velocity field there were two corresponding
 21 eigen values λ_1 and λ_2 . A point in the velocity field was identified as a part of the vortex core
 22 only if both the eigenvalues were negative with the condition $\lambda_1 < \lambda_2$. The center of the vortex
 23 was then the point with the least or the “most negative” value of λ_2 . The contour plots shown
 24 in Figure 6 show the λ_2 variation in the velocity field for two time instants. The vortex center

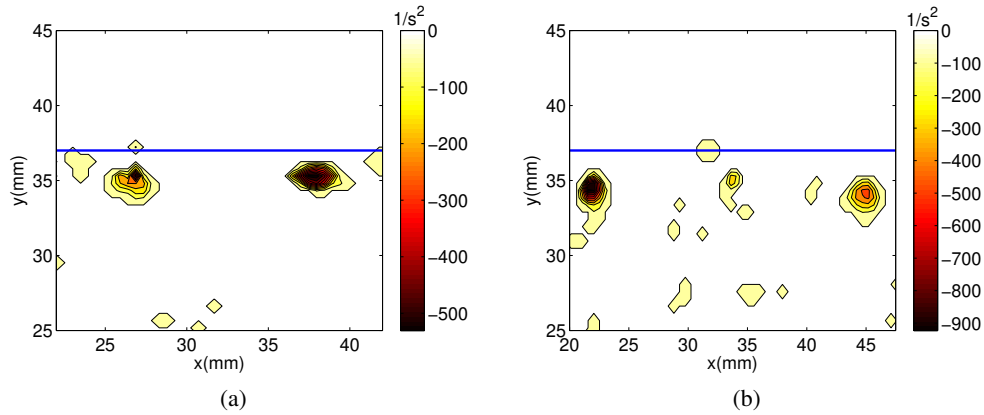


FIG. 6: Contour plots of λ_2 values in the velocity fields for $C_e = 80\%$ and $r_d = 1$ mm at (a), $t = 80$ and (b), 400 ms. The solid line (blue) represents the free surface.

- 1 positions are thus identified at various time instants and their displacement is measured from the
- 2 point of drop deposition.

3. RESULTS AND DISCUSSION

4 Figure 2 shows the top view visualization of film spreading for a drop size of $r_d = 0.97$ mm
 5 with ethanol concentration $C_e = 80\%$. The white particle free regions in the images show the
 6 spreading alcohol film which expands radially. The film continues to expand till about $t =$
 7 150ms, beyond which it retracts. Interestingly, a few time steps after the drop deposition we
 8 observe growing instabilities at the outer periphery of the radially spreading film. As it can be
 9 observed from Figure 2(c), these growing instabilities resemble plumes which merge at later
 10 stages when their mushroom caps touch each other. It is likely that these plumes are an outcome
 11 of a Rayleigh Taylor instability, novel due to their two dimensionality, modulated by surface
 12 tension and viscosity. As seen in Figure 2(d), the film retracts after expanding for some distance
 13 and becoming unstable, possibly due to the surface tension increase at the center of the film due
 14 to the mixing induced by the expanding vortex ring.

15 Figure 3 shows the side view visualizations carried out for an ethanol drop with $r_d=1$ mm and
 16 $C_e=100\%$ where it can be observed that a small fraction of the drop gets pulled along the surface
 17 and spreads on the water layer as a thin film while the remaining portion of the drop floats at the

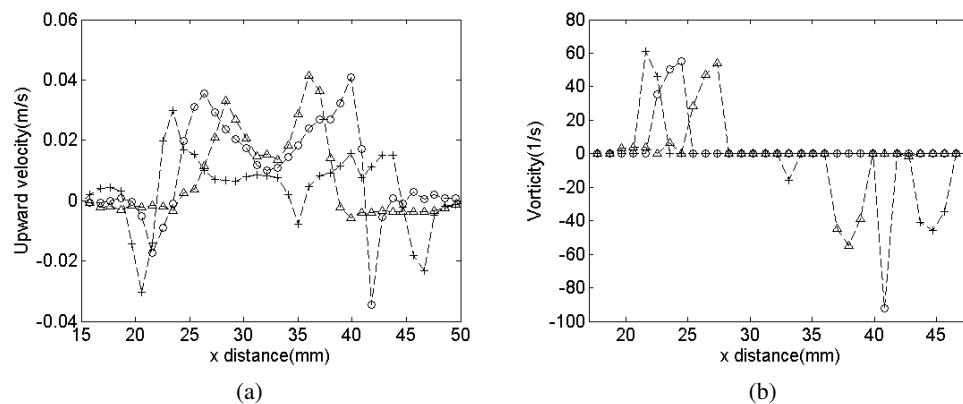


FIG. 7: (a) Variation of the vertical velocity (u_y) along a line passing through vortex centers at times corresponding to those in Figure 5 and (b) Variation of z component of vorticity (ω_z) along the same line at the same times. The symbols represent the data at three time instants after drop deposition: \triangle , $t = 80$ ms; \circ , $t = 240$ ms and $+$, $t = 400$ ms. The point of drop deposition is at $x = 32.16$ mm.

1 center due to buoyancy and negligible mixing. We also observe vortices (see the dashed circles)
 2 traveling below the spreading film, which we infer to be the signature of an expanding vortex
 3 ring. Since the vortex ring occurs at the outer periphery of the expanding film, it appears that the
 4 surface tension difference between the film and the substrate has a role to play in the generation
 5 of vorticity at an interface and the formation of this vortex ring.

6 The velocity fields in the water layer, after the drop is deposited on the water layer for the
 7 spreading of an ethanol film with $r_d = 1.1$ mm and $C_e = 80\%$ are shown in Figure 5 for
 8 three time instants in a vertical plane, as obtained from PIV. On observing the flow field, we
 9 notice the presence of two counter rotating vortices on either side of the point where the drop
 10 was deposited. These vortices are found below the water surface and travel outwards and away
 11 from the point of drop deposition. The vortices observed in Figure 3 are now seen to be counter
 12 rotating, below the free surface and traveling outward indicating that they are the cross section
 13 of an expanding, single vortex ring, expanding along with the film. The figures also show an
 14 upward flow impinging the spreading film at its center, possibly due to the induced velocity of
 15 the expanding vortex ring.

16 Figure 7(a) shows the distribution of the vertical velocity component along a horizontal line
 17 through the center of the vortices in Figure 5 at the same time instants as that in the images of

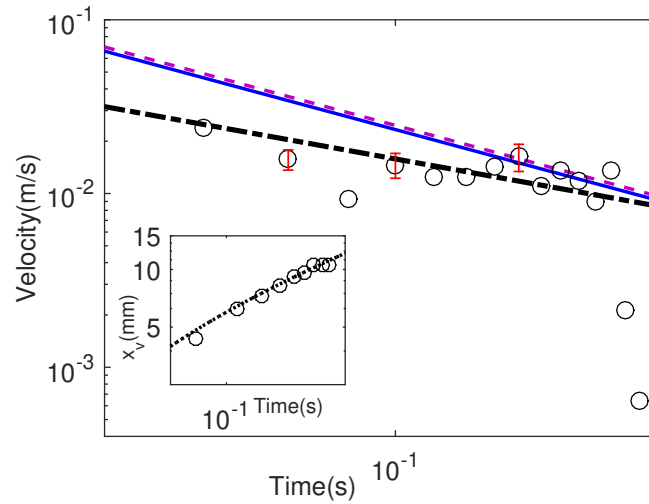


FIG. 8: Variation of the translational velocity of vortices (u_v), the film spreading velocity (u_f) and the vertical component of velocity (u_y) with time for an ethanol drop of $r_d = 1$ mm, $C_e=80\%$ deposited on a 50mm deep water layer. The hollow symbols represent u_y , the dashed line(pink) is $u_v = 4.385t^{-3/4}$, the solid line(blue) is $u_f = 4.15t^{-3/4}$, and the dash-dotted line(black) shows the fit $u_y = 0.005t^{-1/2}$. The inset shows the vortex displacement(x_v) versus time for the same case along with the curve fit $x_v = 17.54t^{0.25} - 3.88$.

1 Figure 5, the vortex centers were identified by the λ_2 criterion (Jeong and Hussain (1995)). Cen-
 2 ters of the vortices can also be identified in Figure 7(a) as the points where the velocity values
 3 change sign. Figure 7(a) shows the development of an upward flow in the bulk with time between
 4 the vortex centres. Figure 7(b) shows the spatial distribution of the z component of vorticity(Ω_z)
 5 at three instants along the centerline of the vortices. We observe that the total vorticity increases
 6 and then plateaus with time. Since there is no vorticity in the stationary water before drop depo-
 7 sition, we hypothesize that this increase and plateauing is because of the vorticity production due
 8 to surface tension gradients at the interface, and its eventual dissipation. Possibly, the vorticity
 9 created at the interface by the gradient of surface tension at the free surface then rolls up into a
 10 vortex ring below the interface.

11 The dimensionless velocity of expansion of the ethanol film at the water surface is given by
 12 Dandekar et al. (2017) as

13

$$Ca_d = \frac{1}{8f^4 r_f^{*3}}, \quad (4)$$

1 where $Ca_d = u_f \mu_d / \Delta\sigma$, the Capillary number, with u_f , the film spreading velocity. Expression
 2 (4) implies that

$$u_f = \frac{0.125}{f^4} \frac{1}{0.83^3} \left(\frac{\Delta\sigma r_d^3}{\mu} \right)^{\frac{1}{4}} t^{-3/4}, \quad (5)$$

3 which is shown as the solid blue line in Figure 7 . The inset in Figure 8 shows the measured
 4 values of the vortex displacement x_v with respect to time for a drop size of $r_d = 1$ mm. The
 5 dotted line in the inset shows the curve fit used to calculate $u_v = dx_v/dt$, the vortex ring
 6 expansion velocity. Figure 8 shows the variation of u_v with time for a given drop size as the pink
 7 dashed line; u_v is found to vary as $u_v = 4.385t^{-3/4}$. Interestingly, the variation of u_v with time
 8 is almost same as that of u_f given by (5). We hence hypothesize that the vortex ring is created
 9 due to the surface tension difference at the edge of the expanding film of ethanol, which causes
 10 the vortex ring to expand in the same way as the film expands.

11 3.1 Scaling for the upward velocity

12 Figure 7 also shows the variation of the upward velocity u_y at the center of the line joining the
 13 two vortex centers with time; u_y varies approximately as $t^{-1/2}$. Since this upward velocity is
 14 possibly the cause of the eventual retraction of the spreading film, due to its role in enhancing
 15 the mixing at the centre of the spreading film, understanding its scaling is important. We now
 16 present a scaling argument for such a variation of u_y .

17 Dimensionally, the vorticity generated due to a surface tension gradient $\Delta\sigma$ across a length
 18 $c_1 r_f$ is expected to scale as

$$\omega = \frac{\Delta\sigma}{c_1 \mu_f r_f}, \quad (6)$$

19 where μ is the dynamic viscosity of the substrate liquid and c_1 a prefactor. If this vorticity is
 20 accumulated in the vortex ring, the circulation around a section of the vortex ring is, $\Gamma = \int_A \omega dA$.

1 For negligible change in the cross sectional area of the vortex ring A then,

$$\Gamma \simeq A\omega, \quad (7)$$

2 which along with (6) implies that

$$\Gamma \simeq \frac{\Delta\sigma A}{c_1\mu_f r_f}. \quad (8)$$

3 The film radius r_f (1) given by Dandekar et al. (2017) is,

$$r_f = \frac{c_2}{f} \left(\frac{\Delta\sigma r_d^3}{\mu_d} \right)^{1/4} t^{1/4}, \quad (9)$$

4 where $c_2=0.83$. Due to the fast spreading of the film on the water layer, negligible mixing occurs,

5 this implies that the film properties will be same as the drop properties. Therefore, $\rho_f = \rho_d$,

6 $\sigma_f = \sigma_d$ and $\mu_f = \mu_d$.

7 Substituting (9) in (8) and replacing μ_f with μ_d results in,

$$\Gamma \simeq \frac{f}{c_3} A \left[\left(\frac{\Delta\sigma}{\mu_d r_d} \right)^3 \frac{1}{t} \right]^{1/4}, \quad (10)$$

8 where $c_3 = c_1 c_2$.

9 The velocity induced at the center of this vortex ring, assuming that the radius of the vortex ring

10 scales in the same way as the film spreading radius r_f given by (9) r_f is

$$u_\Gamma = \frac{\Gamma}{4\pi r_f} \quad (11)$$

11 (Batchelor (2000)). Replacing Γ and r_f in (11) with (10) and (9), the induced velocity can be

12 approximated as,

$$u_\Gamma \simeq \frac{f^2}{c_4} \sqrt{\frac{\Delta\sigma A^2}{\mu_d r_d^3 t}}, \quad (12)$$

1 where $c_4 = c_2 c_3$. The expression (12) can be rewritten as,

$$\frac{u_\Gamma}{u_{\mu\sigma}} = \frac{f^2}{c_4} \sqrt{\frac{t_c}{t}}, \quad (13)$$

2 where $u_{\mu\sigma} = \Delta\sigma/\mu_d$, $t_c = (A^2\mu_d/\Delta\sigma r_d^3)$ and f is given by (2).

3 Figure 8 shows the fit $0.005t^{-1/2}$ plotted along with the measured upward velocity values u_y
 4 at the center of the vortex centerline. It is observed that after the initial rise in the measured
 5 value of u_y due to the drop touching the surface, the experimental u_y follows the $t^{-1/2}$ trend
 6 of the induced velocity u_Γ reasonably well. The dimensionless power law (13) implies that
 7 $u_\Gamma \sim \sqrt{u_{\mu\sigma} u_c}$, where $u_c = A^2/r_d^3 t$. The scaling assumed that A is a constant. However it is
 8 possible that A is a function of other independent parameters. These aspects of the scaling need
 9 to be explained further.

10 4. CONCLUSIONS

11 When a volatile film of ethanol spreads on the surface of a deep water layer from a drop of
 12 ethanol deposited on the free surface, the surface tension gradients create vorticity at the free
 13 surface, which manifests itself in the form of a vortex ring. We show that the velocity of expan-
 14 sion of such a vortex ring scales as $u_v \sim t^{-3/4}$, same as the scaling for the spreading velocity of
 15 the film shown by Dandekar et al. (2017). We also observed that an upward flow, induced by the
 16 expanding vortex ring, was present in the bulk. Based on a dimensional reasoning, we proposed
 17 an expression (6) for the vorticity generated at the interface by a surface tension gradient across
 18 a fraction of the film radius $c_1 r_f$, moderated by the viscosity of the film, which could induce
 19 mixing of the film fluid and the substrate fluid. We use this expression to quantify the circulation
 20 generated at the interface, which possibly manifests itself in the form of a radially expanding
 21 vortex ring. The velocity of the upward flow in the bulk, driven by the expanding vortex ring,
 22 shows a $t^{-1/2}$ power law dependence on time, same as the scaling of the induced velocity by
 23 the vortex ring. These results would be important in understanding the vorticity generation at an
 24 interface in the presence of a surface tension gradient and the associated roll up of the vorticity

1 into a vortex ring.

2 **ACKNOWLEDGMENTS**

3 The equipment used in this work was funded by the grants SR/FST/ETII- 017/2003 and SR/FST/ETII-
4 064/2015 from DST, Government of India.

5 **APPENDIX A. ERROR ANALYSIS FOR PIV EXPERIMENTS**

6 The measurement errors for the vectors obtained from PIV were quantified using the procedure
7 given in Markus et al. (2007), Nobach and Bodenschatz (2009) and Huang et al. (1997). The
8 total error

9 $\epsilon_{total} = \epsilon_{bias} + \epsilon_{ran}$, is a sum of the bias error (ϵ_{bias}) and the random error (ϵ_{ran}).

10 The bias error is due to the loss of particle pairs in the plane of visualization and would lead
11 to a consistent bias towards certain values. The random error

$$12 \quad \epsilon_{ran} = \epsilon_d + \epsilon_{\delta z} + \epsilon_i + \epsilon_s,$$

13 where ϵ_d is the error due to the random changes in particle diameter, $\epsilon_{\delta z}$ the error due to the
14 variation in intensity due to particle motion in a plane perpendicular to sheet, ϵ_i the error due to
15 the image density and ϵ_s the error due to image displacement. ϵ_{bias} , ϵ_d , ϵ_i and ϵ_s were estimated
16 from [Markus et al. (2007), Fig.6.12, Fig.6.14, Fig.6.18, Fig.6.22], where these errors have been
17 plotted against various parameters such as the particle image diameter (d_τ), particle image dis-
18 placement and particle image density (N_I), for different PIV settings. $\epsilon_{\delta z}$ was estimated from an
19 empirical relation provided in Nobach and Bodenschatz (2009) where the constants were chosen
20 on the basis of experimental settings. The values of these errors estimated as described above

ϵ_{bias}	ϵ_d	$\epsilon_{\delta z}$	ϵ_i	ϵ_s
0.010	0.080	0.070	0.020	0.06

TABLE 2: PIV data errors (pixels) through various sources. The estimates were made using the works of Markus et al. (2007), Nobach and Bodenschatz (2009) and Huang et al. (1997)

1 are shown in Table 2. The total random error (ϵ_{ran}) comes out to be 0.230 pixels. Uncertainties
2 in the velocities estimated by each correlation were calculated using DAVIS(Lavision GmbH)
3 which uses the correlation statistics method (Wieneke (2015)). The maximum uncertainty ob-
4 tained in the velocity measurements was 13% of the corresponding velocity.

247 **REFERENCES**

- 248 Adrian, R. and Westerweel, J., *Particle Image Velocimetry*, Cambridge University Press, 2011.
- 249 Agrawal, A. and Prasad, A., Properties of Vortices in the Self-similar Turbulent Jet, *Experiments in Fluids*,
250 vol. **33**, no. 4, pp. 565–577, 2002.
- 251 Bacri, L., Debrgeas, G., and Brochard-Wyart, F., Experimental Study of the Spreading of a Viscous Droplet
252 on a Nonviscous Liquid, *Langmuir*, vol. **12**, no. 26, pp. 6708–6711, 1996.
- 253 Batchelor, G.K., *An Introduction to Fluid Dynamics*, Cambridge Mathematical Library, Cambridge Uni-
254 versity Press, 2000.
- 255 Chong, M.S., Perry, A.E., and Cantwell, B.J., A General Classification of Threedimensional Flow Fields,
256 *Physics of Fluids A: Fluid Dynamics*, vol. **2**, no. 5, pp. 765–777, 1990.
- 257 Dandekar, R., Pant, A., and Puthenveetil, B.A., Film Spreading from a Miscible Drop on a Deep Liquid Layer,
258 *Journal of Fluid Mechanics*, vol. **829**, pp. 304–327, 2017.
- 259 Dussaud, A.D. and Troian, S.M., Dynamics of Spontaneous Spreading with Evaporation on a Deep Fluid
260 Layer, *Physics of Fluids*, vol. **10**, no. 1, pp. 23–38, 1998.
- 261 Ernst, R.C., Watkins, C.H., and Ruwe, H.H., The Physical Properties of the Ternary System Ethyl Alcohol-
262 glycerinwater., *The Journal of Physical Chemistry*, vol. **40**, no. 5, pp. 627–635, 1935.
- 263 Fay, J.A., 1969. The Spread of Oil Slicks on a Calm Sea. Springer US, pp. 53–63.
- 264 Hernandez-Sanchez, J.F., Eddi, A., and Snoeijer, J.H., Marangoni Spreading due to a Localized Alcohol
265 Supply on a Thin Water Film, *Physics of Fluids*, vol. **27**, no. 3, p. 032003, 2015.
- 266 Huang, H., Dabiri, D., and Gharib, M., On Errors of Digital Particle Image Velocimetry, vol. **8**, no. 12, pp.
267 1427–1440, 1997.
- 268 Hunt, J.C.R., Eddies Stream, and Convergence Zones in Turbulent Flows, *Center for Turbulence Research*
269 *CTR-S 88*, pp. 193–208, 1988.
- 270 Jensen, O.E. and Grotberg, J.B., Insoluble Surfactant Spreading on a Thin Viscous Film: Shock Evolution and
271 Film Rupture, *Journal of Fluid Mechanics*, vol. **240**, p. 259288, 1992.
- 272 Jeong, J. and Hussain, F., On the Identification of a Vortex, *Journal of Fluid Mechanics*, vol. **285**, p. 6994,
273 1995.
- 274 Joos, P. and Van Hunsel, J., Spreading of Aqueous Surfactant Solutions on Organic Liquids, *Journal of Colloid*

- 275 *and Interface Science*, vol. **106**, no. 1, pp. 161 – 167, 1985.
- 276 Kim, H., Lee, J., Kim, T.H., and Kim, H.Y., Spontaneous Marangoni Mixing of Miscible Liquids at a Liquid
277 Liquid Air Contact Line, *Langmuir*, vol. **31**, no. 31, pp. 8726–8731, 2015, PMID: 26185919.
- 278 Markus, R., Christian, E.W., Fulvio, S., Christian, J. Kahler.and Steve, T.W., and Jurgen, K., 2007. Particle
279 Image Velocimetry : a practical guide. Springer.
- 280 Nobach, H. and Bodenschatz, E., Limitations of Accuracy in Piv due to Individual Variations of Particle
281 Image Intensities, *Experiments in Fluids*, vol. **47**, no. 1, pp. 27–38, 2009.
- 282 Wieneke, B., PIV Uncertainty Quantification from Correlation Statistics, *Measurement Science and Technol-*
283 *ogy*, vol. **26**, no. 7, p. 074002, 2015.
- 284 Zhou, J., Adrian, R.J., Balachandar, S., and Kendall, T.M., Mechanisms for Generating Coherent Packets of
285 Hairpin Vortices in Channel Flow, *Journal of Fluid Mechanics*, vol. **387**, p. 353396, 1999.